ADVANCED ENERGY MATERIALS

Supporting Information

for *Adv. Energy Mater.*, DOI 10.1002/aenm.202302322

The Impact of Microstructure on Filament Growth at the Sodium Metal Anode in All-Solid-State Sodium Batteries

*Ziming Ding, Yushu Tang, Till Ortmann, Janis Kevin Eckhardt, Yuting Dai, Marcus Rohnke, Georgian Melinte, Christian Heiliger, Jürgen Janek and Christian Kübel**

The Impact of Microstructure on Filament Growth at the Sodium Metal Anode in All Solid-State Sodium Batteries

*Ziming Ding, Yushu Tang, Till Ortmann, Janis Kevin Eckhardt, Yuting. Dai, Marcus Rohnke, Georgian Melinte, Christian Heiliger, Jürgen Janek, Christian Kübel**

Z. Ding, Y. Tang, Y. Dai, G. Melinte, C. Kübel

Institut of Nanotechnology (INT) and Helmholtz Institut Ulm (HIU)
Karlsruhe Institute of Technology (KIT)
76344 Eggenstein-Leopoldshafen, Germany

E-Mail: (Christian.kuebel@kit.edu)

Z. Ding, C. Kübel

Technische Universität Darmstadt
64289 Darmstadt, Germany

C. Kübel

Karlsruhe Nano Micro Facility (KNMF), Karlsruhe Institute of Technology (KIT),
Eggenstein-Leopoldshafen 76344, Germany

T. Ortmann, J.K. Eckhardt, M. Rohnke, J. Janek

Institute for Physical Chemistry
Justus Liebig University Giessen
35392 Giessen, Germany

J.K. Eckhardt, C. Heiliger

Institute for Theoretical Physics
Justus Liebig University Giessen
35392 Giessen, Germany

T. Ortmann, J. K. Eckhardt, M. Rohnke, C. Heiliger, J. Janek

Center for Materials Research (ZfM)
Justus Liebig University Giessen
35392 Giessen, Germany

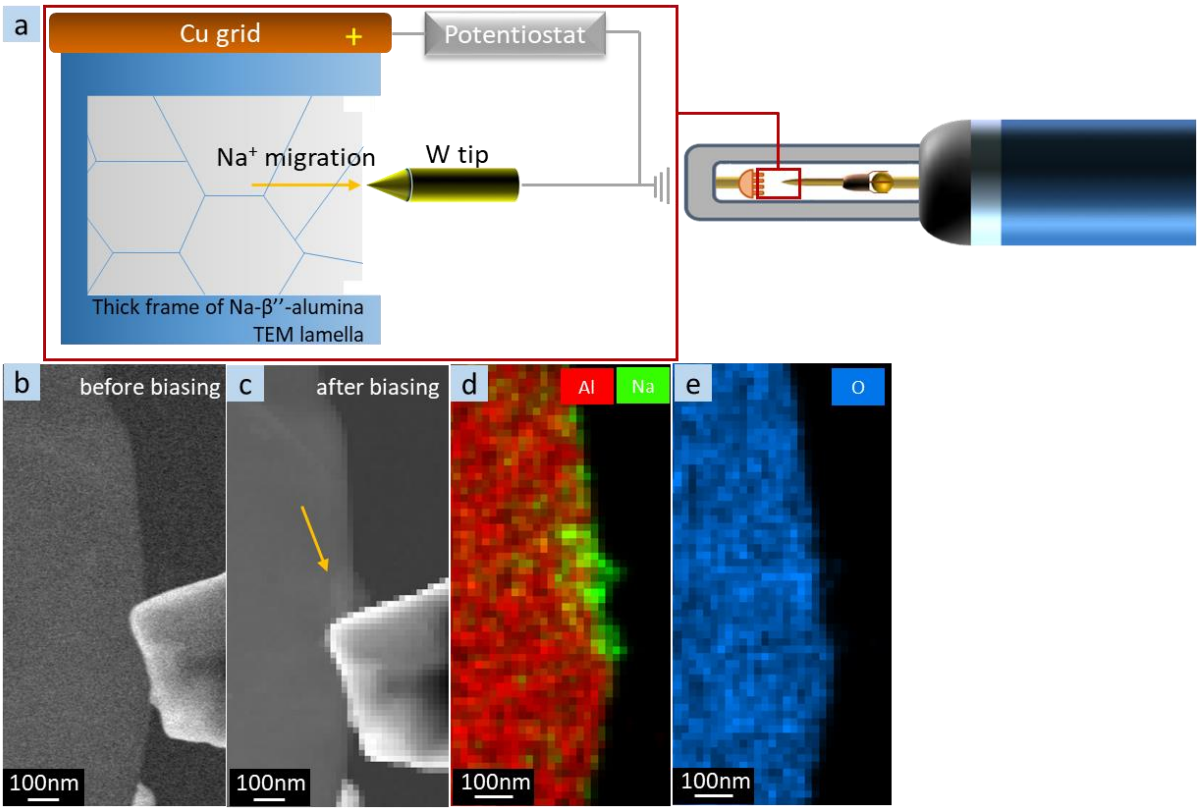

Figure S1. Local electrical contacting of a large Na-β''-alumina grain by the W tip: **a**. schematic of the *in situ* TEM setup. **b**. HAADF-STEM image before biasing. **c**. HAADF-STEM image after biasing. The arrow indicates the position of the Na deposit formed during biasing**.** The W tip was removed after biasing for the acquisition of EDX elemental maps. **d**. EDX maps overlaid for Al (red) and Na (green); **e**. EDX map of O (blue).

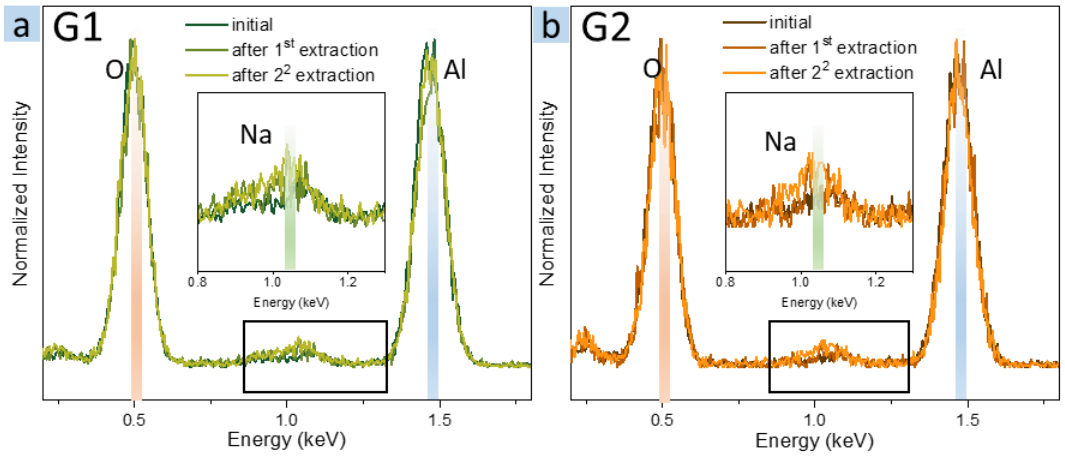

Figure S2. EDX analysis of the grains marked in **Figure 2** before and after Na extraction. **a**. grain 1 (G1, green circle region in **Figure 2**); **b**. grain 2 (G2, orange circle region in **Figure 2**).

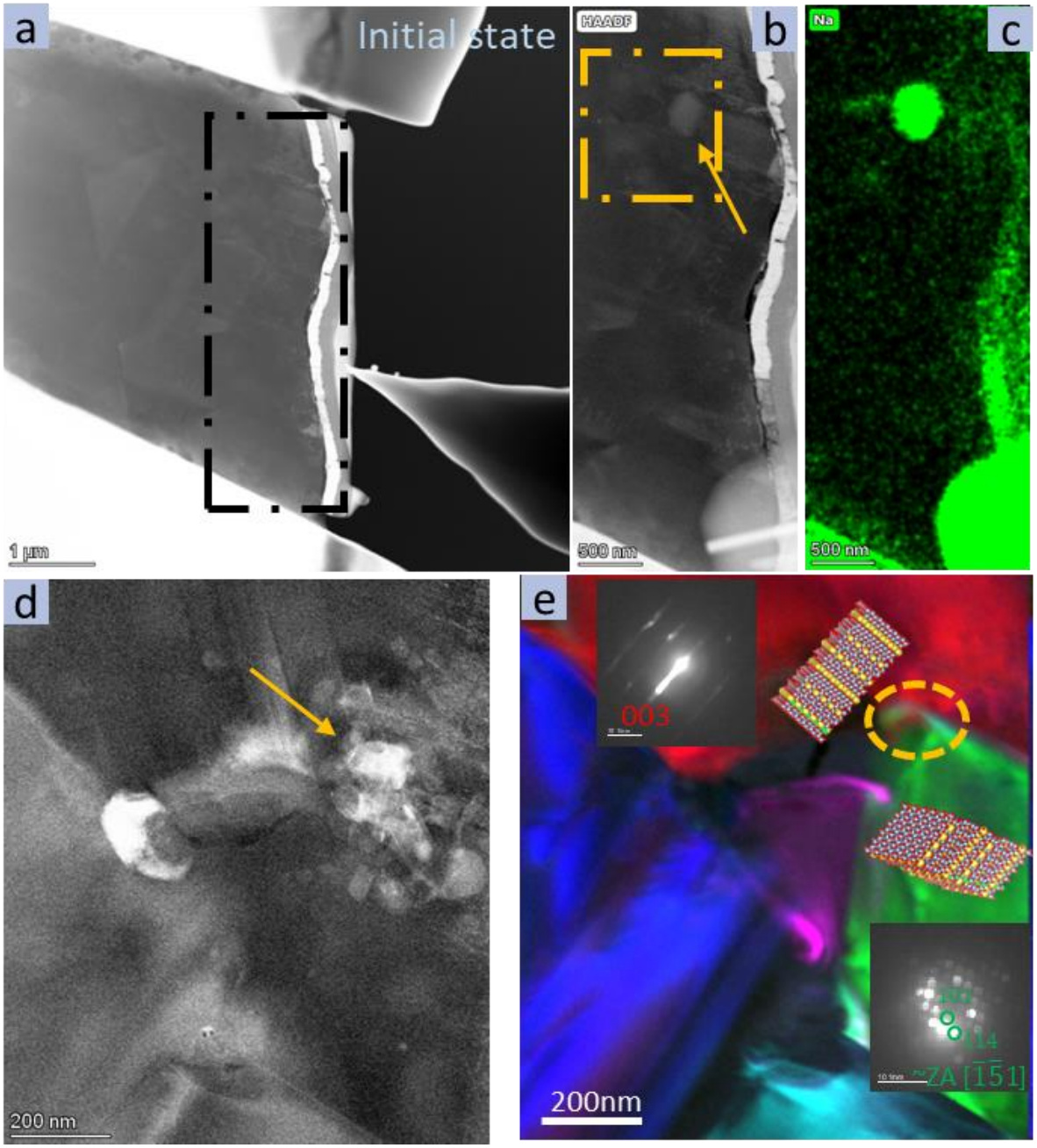

Figure S3. Beam blank reference experiment. **a**. HAADF-STEM image of the initial state; **b. & c**. HAADF-STEM image and EDX Na map after biasing without exposing the sample to the electron beam during biasing; **d**. higher magnification ADF-STEM image of the area marked in yellow in **b**; the yellow arrow points at the Na filament formed. **e**. RGB color coded grain map; the crystal models are shown based on the electron diffractions for those grains obtained by 4D-STEM.

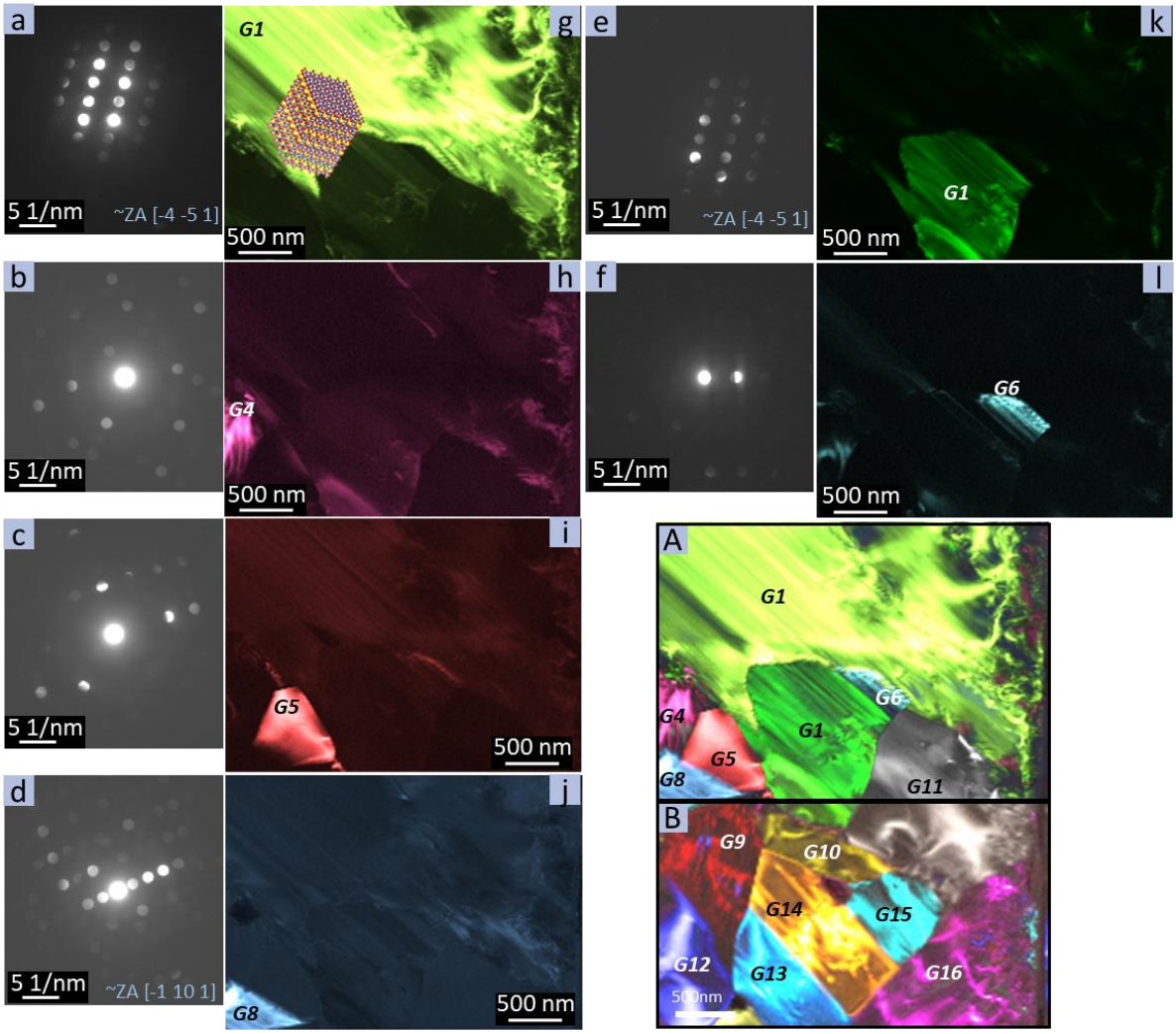

Figure S4. Virtual dark field images (**g – l**) of individual grains in the dark teal dashed rectangle marked area of **Figure 3a** and these grains are numbered following the same sequence. These virtual dark field images were generated from different diffractions (**a – f**) appearing in the 4D-STEM data cube. They are RGB-coded and overlapped to form the grain map: **A.** overlaid images of **g – l**; **B.** overlaid images of **Figure S4 j – r**.

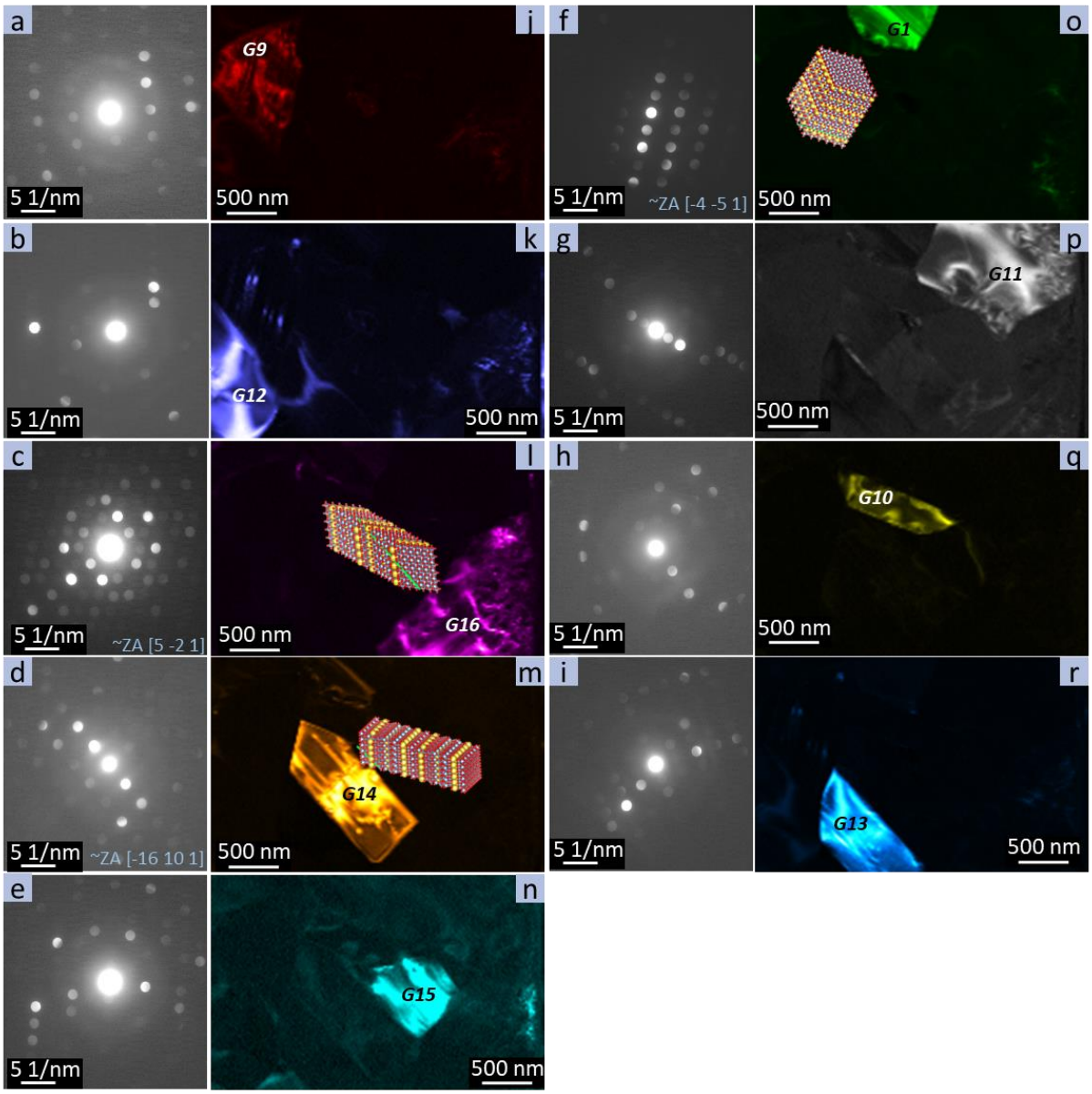

Figure S5. Virtual dark field images (**j – r**) of individual grains in the dark teal dashed rectangle marked area of **Figure 3a**.

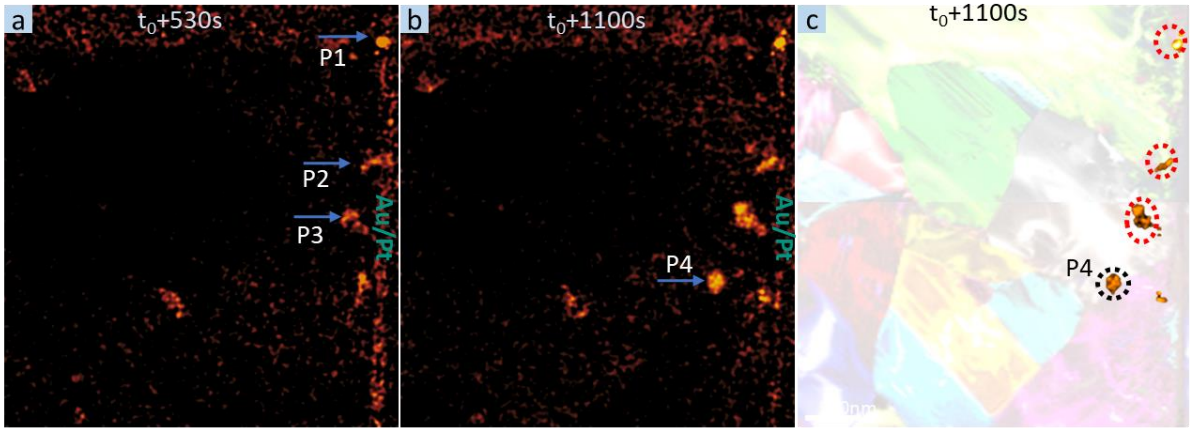

Figure S6. HAADF-STEM difference images to enhance the morphological changes and highlight the position and shape of the Na filaments. From the HAADF-STEM images acquired at t_0 + 530 s (**Figure 3c**) and t_0 + 1100 s (**Figure 3d**) the t_0 image (**Figure 3b**) has been subtracted. **a.** Difference image for t_0 + 530 s with blue arrows indicating Na filaments grown at the interface between Na-β''-alumina and the Au/Pt electrode.; **b.** Difference image at t_0 + 1100 s with the blue arrow indicating a Na filament grown at a GB; **c**. Overlay of **b** and **Figure S3A & B**.

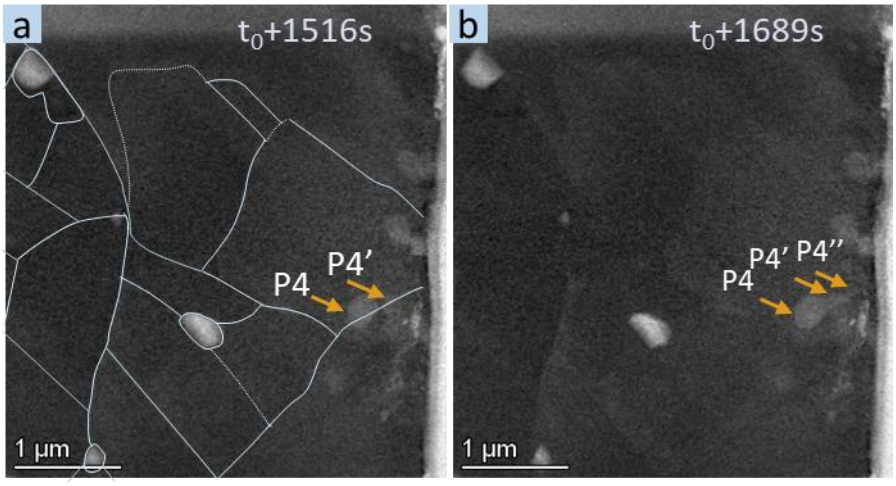

Figure S7. Time series HAADF-STEM images during biasing showing Na filament growth along the GB between grains of G11 and G16. They are between **Figure 3d & e**. **a**. t_0 + 1516 s; **b**. t_0 + 1689 s. Additional filament seeds are indicated by yellow arrows at the position of P4' and P4''.

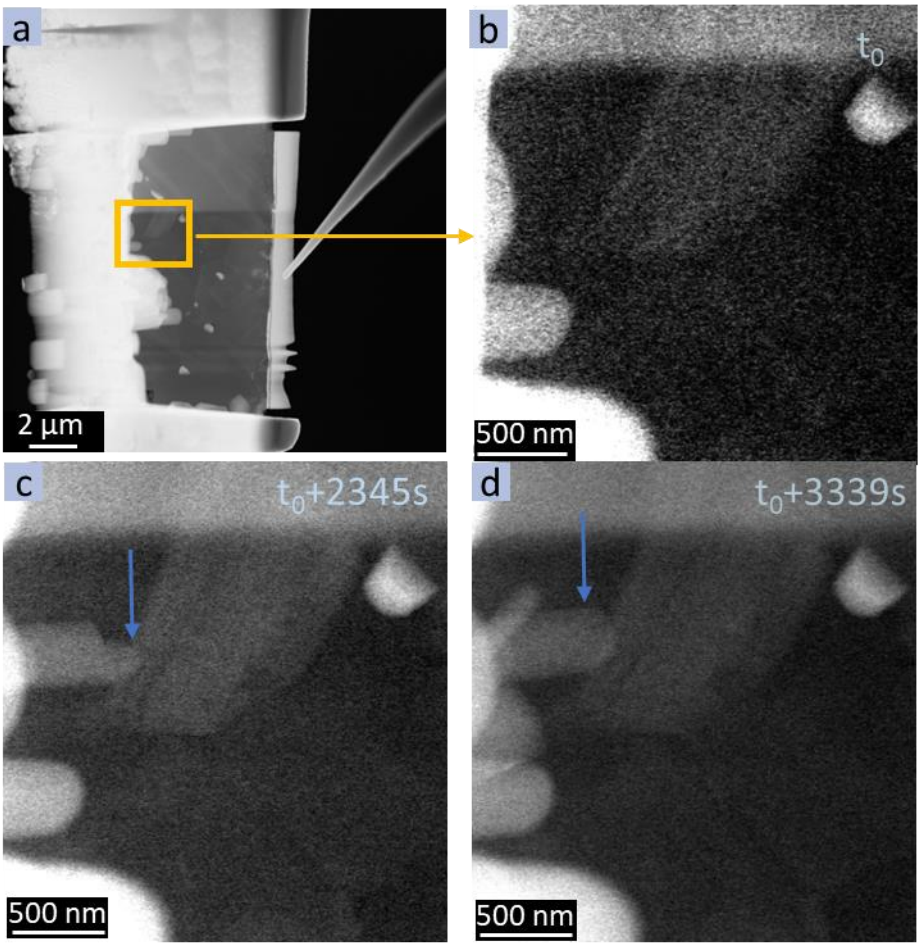

Figure S8. Faceted Na whiskers grown from the backbone region of Na-β''-alumina TEM lamella used in **Figure 3**. **a.** HAADF-STEM image of the overview of the *in situ* setup during the extended biasing; **b.-d.** HAADF-STEM series images of the Na whisker growth at the area indicated by the yellow rectangle in **a**. The blue arrows are indicating the Na whiskers.

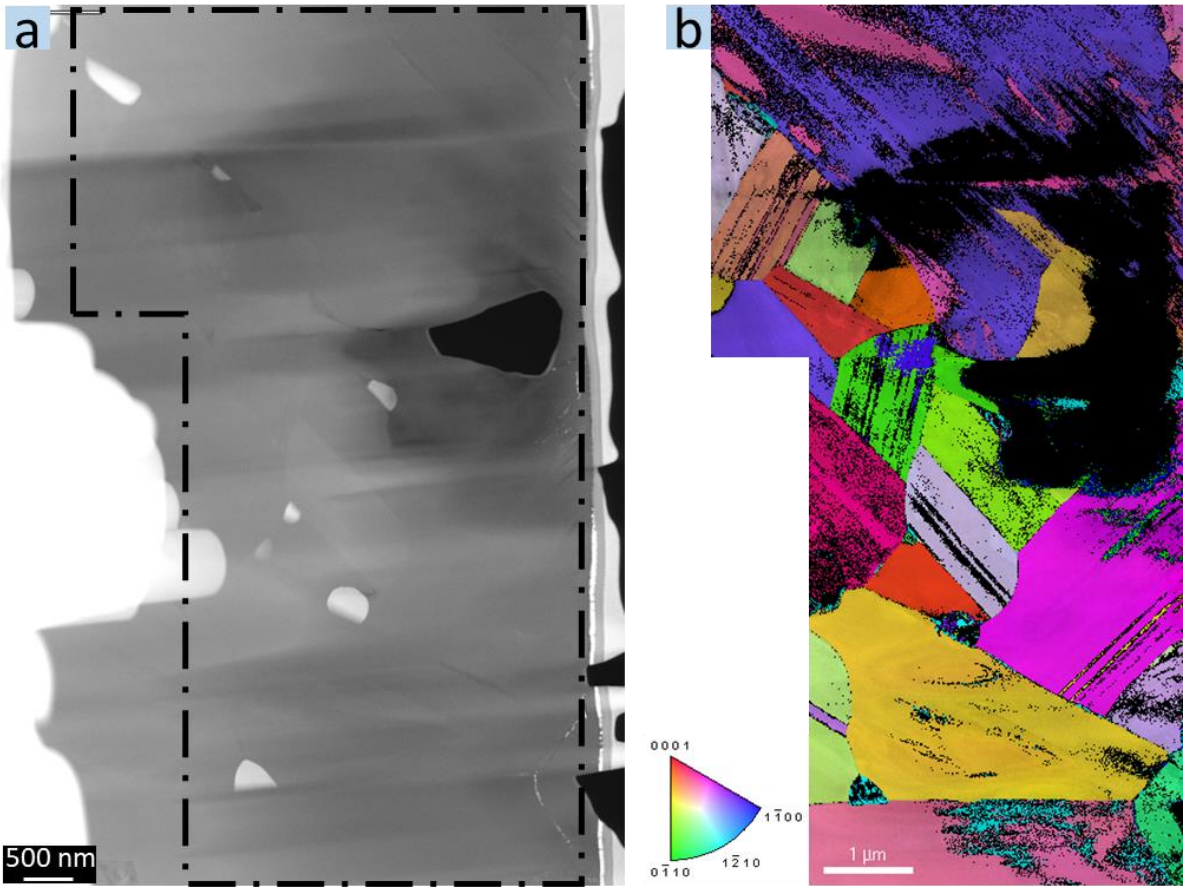

Figure S9. a. HAADF-STEM image of the specimen in Figure 3a after cleaning with FIB; **b.** Overlaid maps of orientation, index, and reliability of the region marked with dot-dash lines in (**a**). The values of index below 600 and reliability under 5 were cut-off.

Since the specimen was furtherly thinned by FIB for a good data set of ACOM, an artificial hole and adjacent damaged region appeared on the specimen. As a consequence, the reliability and index of this region are low and they were removed from the map as shown in **Figure S8**. Nevertheless, the orientation information for each grain is still enough to acquire and illustrate schematically in **Figure 4**.

Table S1. Misorientation between adjacent grains.

GB	Misorientation [°]	Misorientation of Na^+ transport path of adjacent grains [°]
G1/G11	51	14
G9/G5	82	66
G9/G7	88	29
G9/G8	76	66
G9/G10	55	79
G9/G12	71	55
G9/G13	90	53
G9/G14	79	53
G10/G15	35	27
G11/G15	23	10
G11/G16	64	85
G15/G16	63	79
G14/G16	70	89
G13/G16	74	89

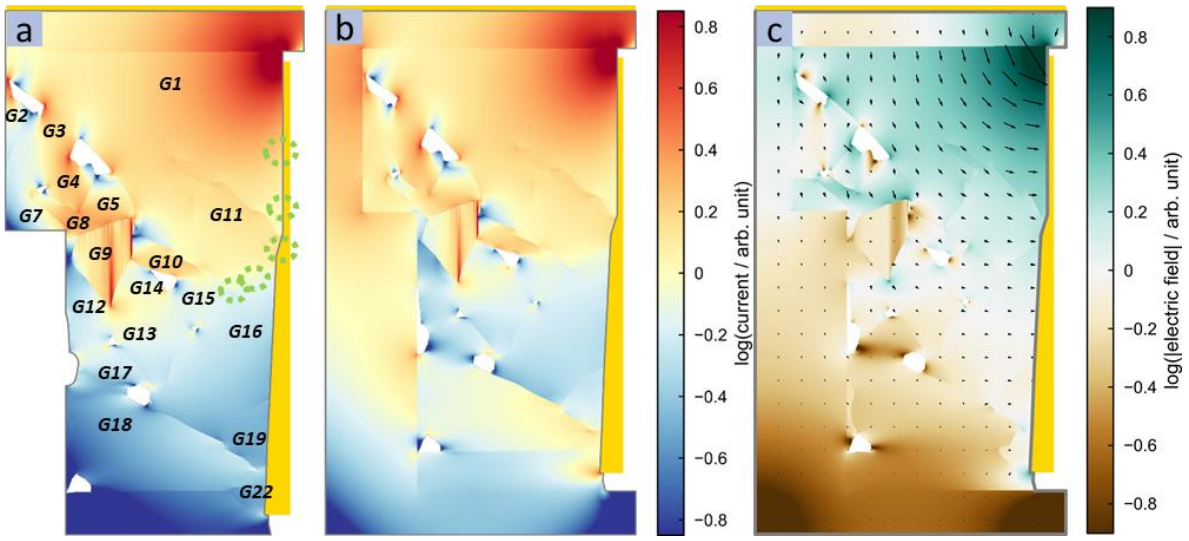

Figure S10. Computational current density distribution for the whole TEM lamella based on the microstructure of the Na-β''-alumina specimen in **Figure 4 and 7a**. The conductivity of individual grains was calculated based on Equation (1). **a**. Current density distribution based on the microstructure of the thin region of the TEM lamella. The thick frame of the TEM lamella was not included. **b**. Current density distribution based on the microstructure of the thin region of the TEM lamella and the thick frame around it. An isotropic effective ionic conductivity was assumed for the thick frame two orders of magnitude lower than in-plane ionic conductivity. The green dashed circles were located at the position of the Na-filament in the experiment. **c.** Electric field distribution based on the microstructure of the thin region of the TEM lamella and the thick frame around it. Isotropic properties were assumed for the thick frame.

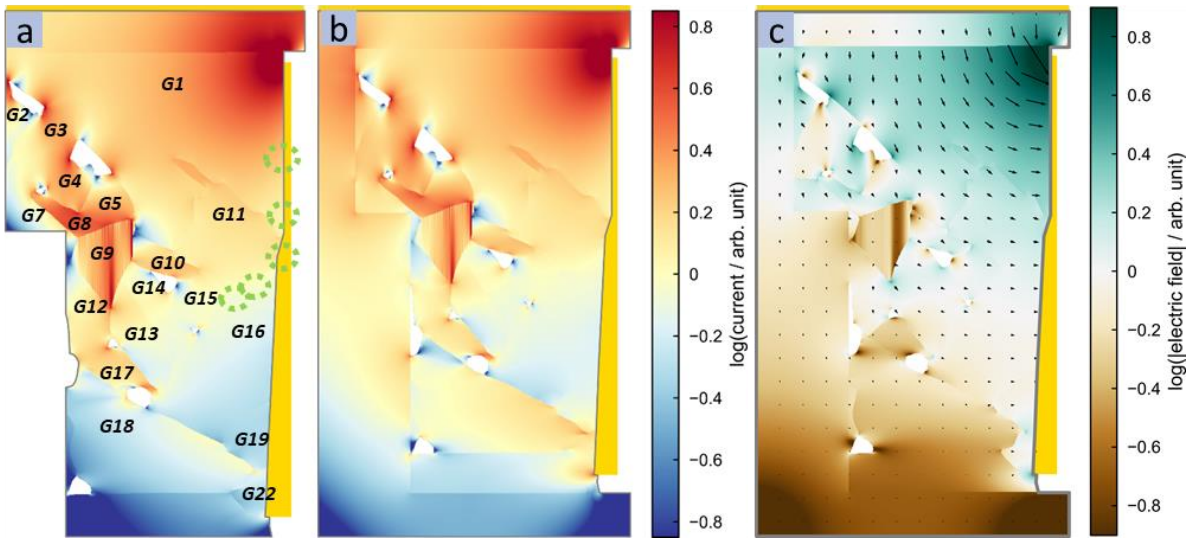

Figure S11. Computational current density distribution of the whole TEM lamella based on the microstructure of the Na-β''-alumina specimen in **Figure 4 and 7a**. The conductivity of individual grains was calculated based on the Equation (2). **a**. Current density distribution based on the microstructure of the thin region of the TEM lamella. The thick frame of the TEM lamella was not included; **b**. Current density distribution based on the microstructure of thin region of the TEM lamella and the thick frame around it. An isotropic effective ionic conductivity was assumed for the thick frame two orders of magnitude lower than in-plane ionic conductivity. The green dashed circles were located at the position of the Na-filament in the experiment. **c.** Electric field distribution based on the microstructure of the thin region of the TEM lamella and the thick frame around it. Isotropic properties were assumed for the thick frame.

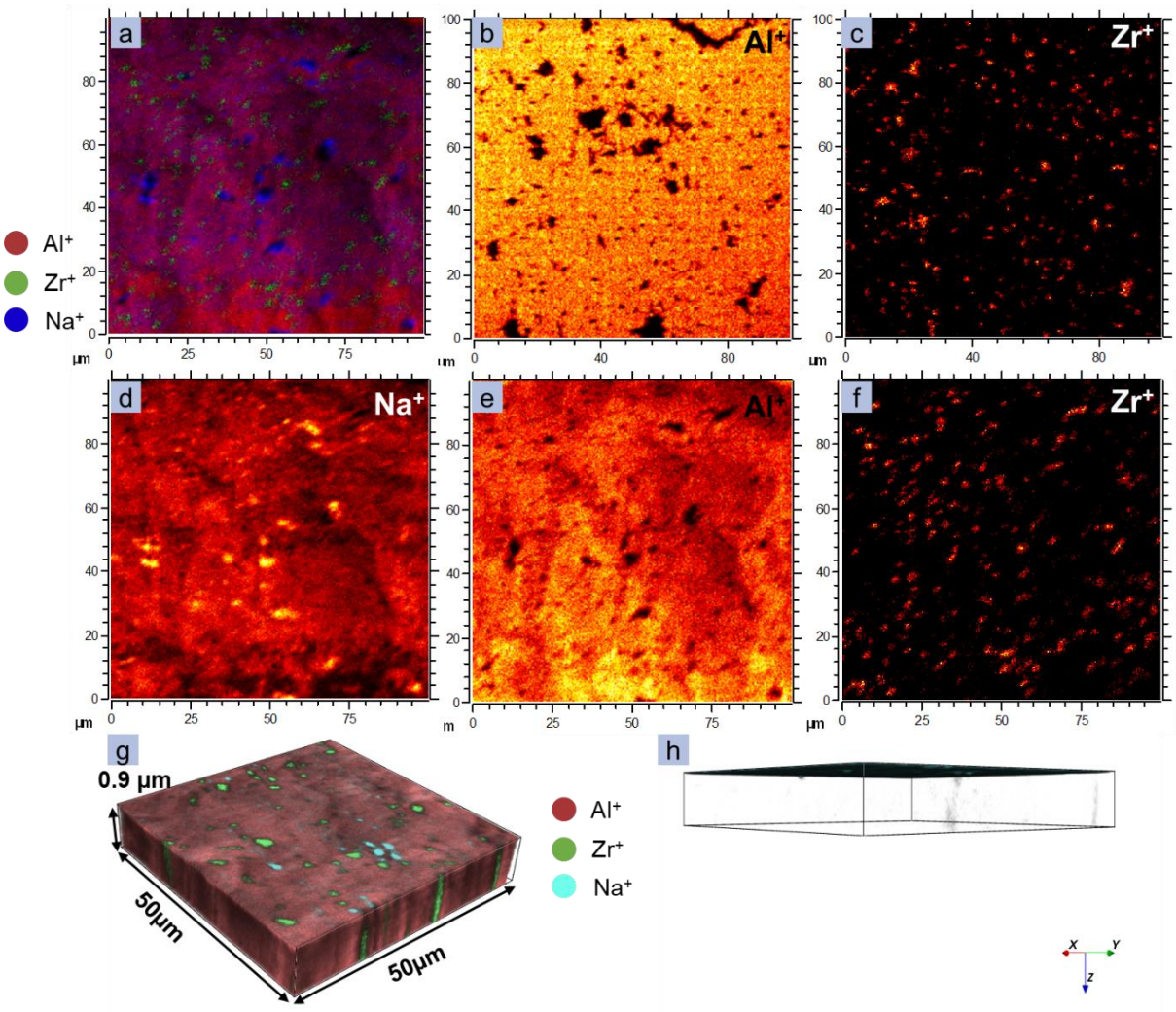

Figure S12. ToF-SIMS elemental analysis of the cycled (**a – c**) and as-prepared (**d – h**) Na-β''-alumina. Cycled sample: **a**. Overlay of Al, Zr, and Na 2D mapping; **b**. Na 2D mapping; **c**. Al 2D mapping; As-prepared sample: **d**. Na 2D mapping; **e**. Al 2D mapping; **f**. Zr 2D mapping; **g**. Overlay of Al, Zr, and Na 3D mapping; **h**. Side view of Na distribution from 3D mapping (**g**).

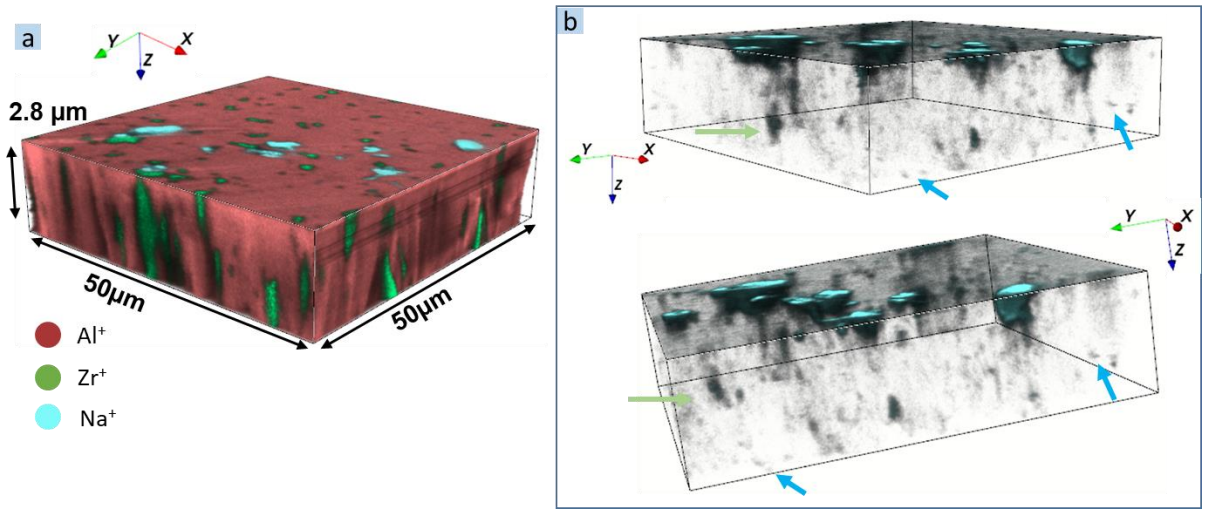

Figure S13. ToF-SIMS maps of another area on the cycled Na-β''-alumina: **a**. ToF-SIMS 3D surface rendering of the sputtered volume of 2.8 µm x 50 µm x 50 µm with an overlay of Al^+, Zr^+, and Na^+; **d**. side view of the Na^+ distribution in 3D

Experimental

Beam-blank reference experiment

Apart from recording the Na-filament growth under long exposure of electron beam during biasing, an electron-beam blank experiment during biasing was also conducted as a reference to eliminate the electron beam influence on the materials. The initial morphology presented in **Figure S3a**. A biasing was applied on the specimen without an electron beam for around 10 min. Then the morphology and Na distribution was acquired as shown in Figure **S3b & c**. Similar to the *in situ* beam-on experiment, a Na particle was found at the GB and a high Na EDX signal was found distributed along GBs. In addition, a crystal mapping of the yellow inset rectangle region of **Figure S3b** was obtained through 4D-STEM as shown in **Figure S3e**. It was found that the GB in which the Na particle appeared belonged to the Type III a2. This is the same as the GB with P4 Na in **Figure 3d**.

Modeling the current density distribution of polycrystalline Na-β''-alumina

To calculate the conductivities σ_i of individual grains in the *x*- and *y*-directions of the sample surface, we considered two different methods based on the orientation of the projected Na^+ ion planes on the sample surface. The current density distributions were calculated in the full

and reduced systems according to both assumptions as shown in **Figure S10 and S11**, respectively. Nevertheless, theses current density distributions exhibit a similar uneven tendency among grains based on both assumptions of the individual conductivities. Therefore, the discussion was mainly based on the first assumption.

1st assumption: The direction of the projection of Na^+ ion plane was only taken into consideration, i.e. the angle θ between projection of Na^+ ion plane and the x-axis of sample surface coordination as shown in **Figure S14**. Therefore, the individual conductivity σ_i can be calculated through **Equation 1**:

$$\sigma_i(\theta) = \begin{cases} \sigma_{op} \cdot |sin\,\theta| + \sigma_{ip} \cdot |cos\,\theta| \\ \sigma_{ip} \cdot |sin\,\theta| + \sigma_{op} \cdot |cos\,\theta| \\ \text{const.} \end{cases} \quad (1)$$

where θ is the angle between the direction of the Na^+ ion plane projection and *x*-axis of sample surface, σ_{ip} is the in-plane Na^+ ion conductivity along the Na plane within the crystal structure, and σ_{op} is the out-of-plane Na^+ ion conductivity.

2nd assumption: The direction of projection of Na^+ ion plane and the contribution of the area of the projection were both considered. The individual conductivities σ_i were calculated following **Equation 2:**

$$\sigma_i(\theta,\, \alpha) = \begin{cases} \sigma_{op} \cdot |sin\,\alpha| \cdot |sin\,\theta| + \sigma_{ip} \cdot (|cos\,\theta| + |cos\,\alpha| \cdot |sin\,\theta) \\ \sigma_{ip} \cdot (|sin\,\theta| + |cos\,\alpha| \cdot |cos\,\theta|) + \sigma_{op} \cdot |\,sin\,\alpha| \cdot |cos\,\theta| \\ \text{const.} \end{cases} \quad (2)$$

where α is the angle between Na^+ ion plane and the surface of Na-β''-alumina.

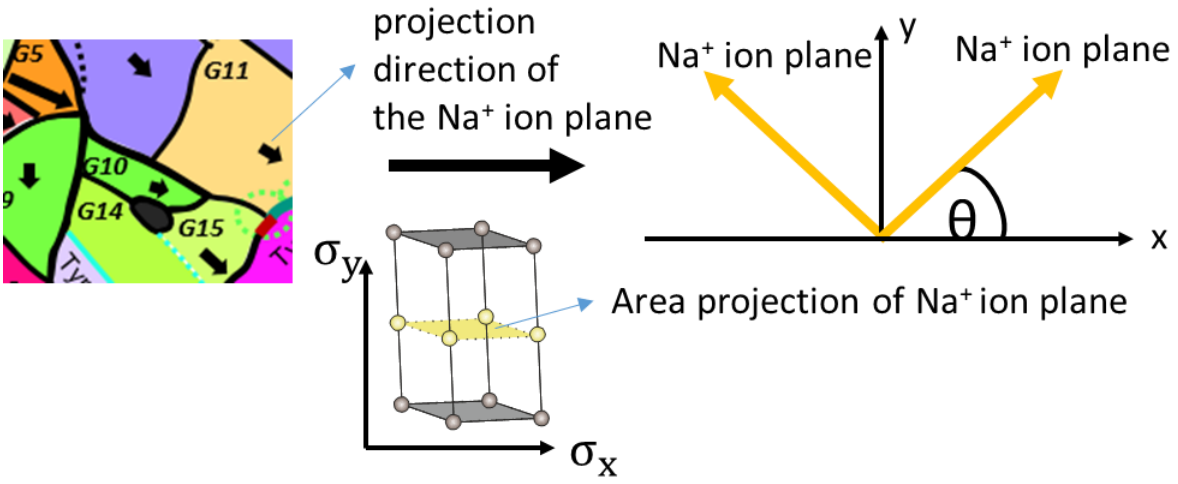

Figure S14. Calculation of the conductivity of individual grains based on the projection of Na^+ ion plane on the surface of Na-β''-alumina (xy-plane). The projection direction of individual Na^+ ion plane was normal to the projection of c-axis of Na-β''-alumina cystall on the Na-β''-alumina sample surface. θ is the angle between the projection direction and *x*-axis of surface of Na-β''-alumina. The area projection of Na^+ ion plane was dependent on the angle α between Na^+ ion plane and the sample surface.

Post mortem ToF-SIMS characterization on the cycled Na-β''-alumina

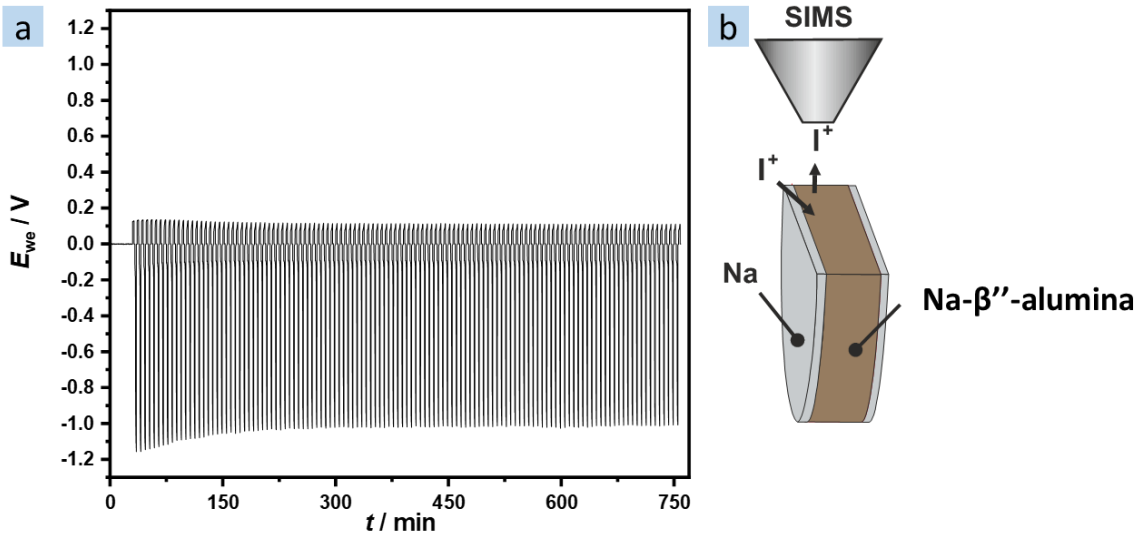

Figure S15. Na|Na-β''-alumina|Na symmetric cell was cycled at area current density of 260 μA/cm^2 for working electrode and 240 μA/cm^2 for counter electrode till 250 cycles.

2 min per cycle, 1 min rest before next cycle; **a**. The voltage of working electrode vs. time profile; **b**. The geometrical configuration of cycled Na-β''-alumina pellet for SIMS characterization.